Original article

Nutthira Pakkang, Manish Kumar, Shogo Taira, Keiichi Koda, Kengo Shigetomi and Yasumitsu Uraki*

Preparation of kraft lignin-based activated carbon fiber electrodes for electric double layer capacitors using an ionic liquid electrolyte

https://doi.org/10.1515/hf-2019-0291
Received November 20, 2019; accepted March 19, 2020; published online May 30, 2020

Abstract: This article demonstrates the development of activated carbon fiber electrodes produced from hardwood kraft lignin (HKL) to fabricate electric double layer capacitors (EDLCs) with high energy and power densities using an ionic liquid (IL) electrolyte. A mixture solution of HKL, polyethylene glycol as a sacrificial polymer, and hexamethylenetetramine as a crosslinker in dimethylformamide/acetic acid (6/4) was electrospun, and the obtained fibers were easily thermostabilized, followed by carbonization and steam activation to yield activated carbon fibers (ACFs). The electrochemical performance of EDLCs assembled with the ACFs, 1-ethyl-3-methylimidazolium tetrafluoroborate ($EMIBF_4$) as an IL electrolyte and a cellulosic separator was insufficient due to the low conductivity of the electrode. The conductivity of the electrode was improved successfully by spraying conductive carbon black (CB) onto the fibers mat during electrospinning. The CB containing electrodes with improved conductivity gave the resulting EDLCs a higher electrochemical performance, with an energy density of 91.5 Wh kg^{-1} and a power density of 76.2 kW kg^{-1}.

Keywords: conductive carbon black; electric double layer capacitor; hardwood kraft lignin; ionic liquid electrolyte.

***Corresponding author: Yasumitsu Uraki**, Research Faculty of Agriculture, Hokkaido University, Sapporo, 060-8589, Japan, E-mail: uraki@for.agr.hokudai.ac.jp
Nutthira Pakkang, Manish Kumar and Shogo Taira: Graduate School of Agriculture, Hokkaido University, Sapporo, 060-8589, Japan
Keiichi Koda and Kengo Shigetomi: Research Faculty of Agriculture, Hokkaido University, Sapporo, 060-8589, Japan

1 Introduction

Renewable materials have attracted much attention as alternatives to diminishing fossil resources due to environmental concerns (Den et al. 2018; Ganewatta et al. 2019; Szabó et al. 2019). Among these materials, lignin is a promising component of wood-based biomass because of its high carbon content and large abundance after cellulose (Cline and Smith 2017; Kołodyńska et al. 2016). Large amounts of technical lignin, especially kraft lignin, are produced as a byproduct in pulp and paper industries and are mostly incinerated as fuel (Lora 2008; Milotskyi et al. 2019; Sixta 2008; Thakur et al. 2014; Tuck et al. 2012). On the other hand, such technical lignins show high resistance against thermal decomposition to give a high yield of char. Based on the characteristic of lignins, carbonaceous materials such as carbon fibers and activated carbon fibers (ACFs) were produced from organosolv and kraft lignins (Kadla et al. 2002; Norberg et al. 2012; Uraki et al. 1995, 2001). The current research on the lignin conversion to the carbonaceous material has focused on the preparation of electrodes for the energy storage device, e. g., electric double layer capacitor (EDLC) (Espinoza-Acosta et al. 2018; Kumar et al. 2019). Several attempts have also been made to improve the electrochemical performance of lignin-based EDLCs: e. g., increasing the specific surface area of the electrode by producing sub-micron to nano-fibers for increasing in active sites and specific capacitance (Ago et al. 2016; Park et al. 2019), improving the conductivity by adding conductive materials (Kiseleva et al. 2018; Saha et al. 2014), and increasing the voltage window by using ionic liquid (IL) electrolytes (De Vos et al. 2014; Mousavi et al. 2016). Among the improved electrodes, Lei et al. (2017) reported a lignin/PAN-based electrode with the highest specific capacitance of 1760 F g^{-1}, but the energy density (47.8 Wh kg^{-1}) and power density (0.8 kW kg^{-1}) were not impressive. In the design of EDLC electrodes, improved energy and power densities are the most important electrochemical parameters, rather than the specific

capacitance (C). Wang et al. (2016) reported the lignin-based EDLC with the highest reported value of energy and power densities (56.6 Wh kg^{-1} and 114 kW kg^{-1}, respectively) which was fabricated from a lignin/SiO_2-derived electrode and an IL electrolyte.

You et al. (2015) reported the lignin-based EDLC electrode with significantly high energy density (42 Wh kg^{-1}) and power density (91 kW kg^{-1}) using an organic electrolyte, where the electrode was prepared from ACFs of hardwood acetic acid lignin. You et al. (2016a) also demonstrated the preparation of EDLC with high packaged energy and power densities, which were estimated based on the total mass of the EDLCs, including the outer packaging. As the EDLC comprised of multiple cells, it was termed as Tandem-EDLCs. The objective of the current study is to achieve EDLC with high energy density using an IL electrolyte based on a single cell (a pair of electrodes).

Herein, the relationship between EDLC performance and electrolyte is described in detail. The formulas for energy density (E) and power density (P) are expressed as $E = 1/8\ CV_{max}^2$ and $P = i(V_{max} - V_{drop})^2/2\ mV_{drop}$, respectively, where C is the specific capacitance, V_{max} is the maximum potential window, i is current, V_{drop} is the voltage drop at the beginning of discharge, and m is the total mass of the pair of electrodes (Kim et al. 2013). Aqueous electrolytes (KOH or H_2SO_4) have a narrow potential window (0–1 V) (Daraghmeh et al. 2017; Gao et al. 2012) and organic electrolytes have potential windows of 0–3.0 V (Mhamane et al. 2013; You et al. 2015), while ILs have potential windows wider than 3.5 V (Hayyan et al. 2013; Ramachandran and Wang 2018). The advantages of using ILs, in addition to the larger potential window, are their high electrochemical & thermal stabilities and high ionic conductivity (De Vos et al. 2014). ILs are thus believed to be promising electrolytes for high energy density electric double layer capacitors (EDLCs).

ILs have larger molecular sizes than aqueous and organic electrolytes (as in Figure 1); therefore, the electrodes for EDLCs using IL electrolytes require larger pore sizes (Wang et al. 2017). However, when the pore size is too large, the capacitance decreases according to the equation $C = \varepsilon A/d$, where C is the capacitance, A is the electrode surface area, d is a distance between the electrolyte and the pore wall of the electrode, and ε is the dielectric constant of the electrolyte (Chmiola et al. 2006). Therefore, the smallest acceptable value of d is important to maintain as high C value as possible. To make pores suitable in sized and distribution in the electrode, hardwood kraft lignin (HKL) was mixed with polyethylene glycol (PEG), which acts as a sacrificial polymer and an agent to improve the spinnability during electrospinning (Salmani and Nouri 2016). When an ACF mat is prepared from the mixture via electrospinning, thermostabilization, carbonization, and steam activation, the well-dispersed PEG in HKL is expected to be easily burned off, resulting in the formation of pores with controlled size and distribution.

In several articles (Deng et al. 2013; You et al. 2015, 2016a), electrodes were fabricated by mixing crushed electrospun carbon fiber mats with conductive materials, such as conductive carbon black (CB) and carbon nanotubes, to increase the conductivity of the electrode. However, this procedure is tedious. Therefore, the ACF mats are used directly as an electrode in an EDLC. As anticipated, the direct use of the HKL-based ACF mat as an electrode results in low electrochemical performance due to the low conductivity. This work demonstrates a modified strategy to embed conductive CB into HKL-electrospun fiber mats. After carbonization and activation, the mats were directly used as electrodes, and the resulting EDLCs showed improved electrochemical performance.

2 Materials and methods

2.1 Materials

Black liquor from hardwood kraft pulping was supplied by Nippon Paper Industries Co., Ltd., Tokyo, Japan. HKL was isolated from the black liquor by precipitation using 0.1 M hydrochloric acid (HCl), followed by filtration and washing with distilled water. Finally, the wet HKL was freeze-dried (Aso et al. 2013).

Hydrochloric acid (HCl), polyethylene glycol with 500 kDa (PEG), acetic acid (AcOH), dimethylformamide (DMF), hexamethylenetetramine

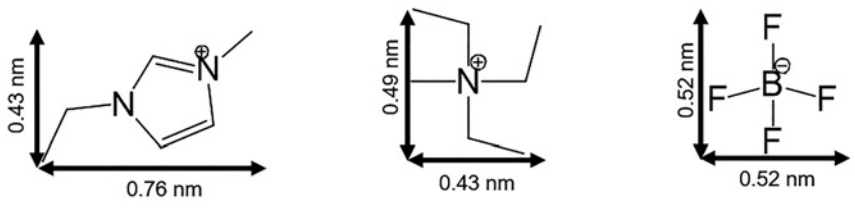

Figure 1: Anion and cation sizes of ionic liquid ($EMIBF_4$) and organic ($TEMABF_4$) electrolytes.

(hexamine; Hex), and propylene carbonate (PC, battery grade) was purchased from FUJIFILM Wako Pure Chemical Industries, Co., Ltd., Osaka, Japan. Triethylmethylammonium tetrafluoroborate ($TEMABF_4$) and 1-ethyl-3-methylimidazolium tetrafluoroborate ($EMIBF_4$) (Figure 1) were purchased from Tokyo Chemical Industry Co., Ltd. Conductive CB was purchased from Alfa Aesar, Heysham, UK (Super P conductive, 99+%). All chemicals were used as received without further purification. Aluminum foil (0.1 mm in thickness) was purchased from Nilaco Corporation (Tokyo, Japan). Cellulosic separator (Type-A sheet) was supplied by Mitsubishi paper Mills Ltd. Tokyo, Japan.

2.2 Electrospinning of HKL

HKL was mixed with PEG at an HKL/PEG weight ratio of 99/1 and 95/5 in dimethylformamide (DMF) via vigorous stirring at 60 °C for 1 h to prepare 35, 40, and 45 wt.% solutions. Separately, mixtures of HKL/PEG with the same ratios as above were mixed with Hex (10 wt% based on the mixtures) in the binary solvent DMF/AcOH (with a weight ratio of 6/4) and then stirred for 2 h at 60 °C to yield 35 wt% solutions. The resulting solutions were electrospun using the following conditions: a voltage of 18 kV, a solution flow rate of 1.2 ml h^{-1}, and a tip-collector distance of 13 cm. The electrospinning machine was manufactured in the Machinery Laboratory of the Faculty of Science at Hokkaido University.

During the electrospinning of HKL/PEG/Hex, a 1 wt% suspension of conductive CB in acetone was sprayed several times until the mass of CB reached 1 wt% and 5 wt% on the electrospun fiber mats.

2.3 Thermostabilization, carbonization, and activation

The electrospun fiber mats were heated in the air from room temperature (RT) to 250 °C at a heating rate of 0.5 °C min^{-1} and 2 °C min^{-1}. The temperature was held for 1 h before cooling down to RT. The obtained thermostabilized fiber mat was carbonized under N_2 stream (flow rate, 0.5 L min^{-1}) by heating from RT to 900 °C at a heating rate of 3 °C min^{-1}, followed by holding the temperature for 1 h. Steam activation was carried out after carbonization without cooling, according to the methods of a previous report (You et al. 2016b). The resulting lignin-based ACFs derived from HKL/PEG 99/1 and 95/5 without CB are referred to as ACF-99/1 and ACF-95/5, respectively. When 1 wt% CB is embedded on the fiber mat with a blending ratio of 99/1, the resultant ACF is abbreviated as ACF-99/1-1CB. Similarly, the other materials are abbreviated as ACF with the blend ratio and CB content.

2.4 EDLC assembly

ACF mats, aluminum sheets, and a cellulosic separator were cut into circles 16 mm in diameter. At least two ACF circle sheets with the same weight (within 0.1 mg deviation) were selected as a pair of electrodes. Each part of the electrodes was dried *in vacuo* for 2 h. The EDLCs were assembled in a two-electrode measurement cell (2E-CELL-SUS, Eager Corporation, Osaka, Japan) for evaluating the electrochemical performance as follows. An aluminum sheet, an ACF mat electrode and the cellulosic separator were successively placed on the bottom of the measurement cell. Then, 2–3 drops of the $EMIBF_4$ IL electrolyte were poured on the separator, and then another ACF mat electrode and aluminum sheet were successively placed on top of the separator. Thus, the separator with IL electrolyte was sandwiched between a pair of ACF mat electrodes. Finally, a stainless-steel disk was placed as a spacer on the aluminum sheet, and the assembled EDLC was tightly pressed using a spring. This assembly process was carried out in a glove box under N_2 atmosphere. Similarly, EDLCs using ACF mats with $TEAMBF_4$/PC as an organic electrolyte were assembled as reference EDLCs. The electrochemical performance of the EDLCs was evaluated by using an electrochemical workstation (Autolab PGSTAT302N FRA32M, Metrohm Autolab B.V., Tokyo, Japan) in air and argon atmospheres.

2.5 Electrochemical measurements

Cyclic voltammetry (CV) was measured with a scan rate of 0.05 V/s and a potential window of 0 to 3.5 V, and the specific capacitance was calculated according to Equation (1) (Pandit et al. 2017)

$$C_s = \frac{1}{mv(V_f - V_i)} \int_{V_i}^{V_f} I(V)dV \quad (1)$$

where C_s indicates the specific capacitance (F/g), V_f and V_i, respectively, are the final and initial voltage (V), v is the scan rate (V/s), $\int_{V_i}^{V_f} I(V)dV$ is the area under the CV curve, using Origin Pro software (version 8; OriginLab, Northampton, MA, USA), and m is the total weight (g) of the materials of the two electrodes. Galvanostatic charge/discharge (GCD) measurements were carried out at a current density of 1 A g^{-1} within the same voltage range. The specific capacitance was actually determined from the GCD curves using the following formula:

$$C_s = \frac{4i}{m \cdot dV/dt} \quad (2)$$

where i is the applied current, m is the weight of the two electrodes (g), and dV/dt is the slope obtained by fitting a straight line to the discharge curve over the range of 60–45% of V_{max}, where V_{max} is the maximum value of the operating potential window (You et al. 2015). Electrochemical impedance spectroscopy (EIS) experiments were carried out at open circuit potential with an amplitude of 10 mV and a frequency range of 100 kHz to 1 Hz. The charge transfer resistance (R_c) and intrinsic resistance (R_i) can be calculated from the diameter of the semicircle and the intercept on the Z′ axis in the Nyquist plot, respectively. The energy density (E) and the power density (P) was estimated according to Kim et al. (2013).

2.6 Other instrumental analyses

The morphology of the fibers was observed under an optical microscope (Violet laser color 3D profile microscope VK-9500, Keyence Japan, Osaka, Japan) and a field emission-scanning electron microscope (FE-SEM; JSM-6301F, JOEL Ltd., Tokyo, Japan) at an accelerating voltage of 5 kV after gold sputtering. The average diameter of 20 fibers was measured by taking five points on a single fiber.

N_2 adsorption/desorption was measured using a surface area analyzer (Autosorb-1, Quantachrome, Tokyo, Japan) at –196 C. The specific surface areas were calculated from N_2 adsorption isotherms in the relative pressure (P/P_0) range of 0.02 to 0.30 by using the Brunauer, Emmett, and Teller (BET) model. The ratios of the internal to external surface areas in the relative pressure range of 0.2~5 were calculated according to the *t*-plot method (You et al. 2015). The

internal and external areas were calculated based on the ratios and BET surface areas. The average pore sizes, cumulative surface areas, and pore size distributions were calculated from the adsorption isotherms based on quenched solid density functional theory (QSDFT) (Neimark et al. 2009).

The surface resistance of the ACF mats was measured by using a low resistivity meter (Loresta-AX-MCP-T370, Mitsubishi Chemical Analytech, Kanagawa, Japan). ACF mats 1 mm in thickness were cut into 2 × 2 cm pieces. The resistivity was measured by pushing the probe with a linear 4-pin onto the surface of the mats at five different positions and the average resistances were calculated.

Elemental analyses of the ACF mat on carbon, hydrogen, and nitrogen were performed using a Micro CORDER JM10 (J-Science Lab Co., Ltd, Kyoto, Japan). Raman spectra were recorded with a Raman Renishaw InVia Reflex apparatus (Renishaw PLC, United Kingdom), equipped with the 532 nm laser using an objective lens of 20x. Raman scattering was obtained on crushed ACF samples with an exposure time of 10 s, laser power of 10%, and spectra range of 1000–2000 cm^{-1}.

3 Results and discussion

3.1 Electrospun HKL/PEG-based ACF mat

Table 1 shows that the 35 wt% HKL/PEG solution gave mats comprised of the thinnest fibers, suggesting that lower concentrations contributed to finer fiber formation. This HKL/PEG fiber mat was subjected to thermostabilization for suppressing the fibers from fusing with each other at the elevated temperatures of the carbonization process (Braun et al. 2005; Kadla et al. 2002; Luo et al. 2011; Uraki et al. 1995). This mat required a heating rate lower than 0.5 °C min^{-1} for complete thermostabilization. Extended thermostabilization (e. g. at the heating rate of 0.1 °C min^{-1} for several days) was not assumed viable. Therefore, hexamethylenetetramine (hexamine; Hex), which is a well-known crosslinker for phenol-formaldehyde resins, was added to the HKL/PEG mixture to accelerate the thermostabilization (You et al. 2015). Since the crosslinking reaction proceeded in an acidic media, AcOH was also added to the DMF solution. The resultant solution was subjected to electrospinning, resulting in high spinnability and uniform fibers. The fiber mats prepared from the HKL/PEG/Hex mixtures (99/1/10 and 95/5/10) (as in Figure 2a) in the binary solvents were easily thermostabilized in the air at a heating rate of 2 °C min^{-1} (Figure 2b). The thermostabilization was completed in 3 h at this heating rate.

The thermostabilized mats were then carbonized and successively steam activated for 1 h to obtain ACF mats. Microscopic images (e. g., Figure 2c) show that the

Table 1: Electrospinning conditions and average diameter of electrospun fibers before and after thermostabilization at 2 °C min^{-1}.

Entry	Samples	Solvent	Solution conc. (wt%)	Hex. conc. (wt%)	Diameter (μm)		
					Before[a]	After[b]	Activation
1	99/1[c]	DMF	35		0.48 ± 0.12	–	–
2	99/1[c]	DMF	40		0.53 ± 0.14	–	–
3	99/1[c]	DMF	45		1.24 ± 0.21	–	–
4	95/5[d]	DMF	35		0.57 ± 0.08	–	–
5	95/5[d]	DMF	40		0.62 ± 0.09	–	–
6	95/5[d]	DMF	45		1.66 ± 0.18	–	–
7	99/1[c]	DMF/AcOH	35	10	0.65 ± 0.18	0.60 ± 0.10	0.56 ± 0.09
8	95/5[d]	DMF/AcOH	35	10	0.97 ± 0.09	0.76 ± 0.15	0.71 ± 0.10
9	95/5[d] -1CB	DMF/AcOH	35	10	1.07 ± 0.16	0.95 ± 0.14	0.92 ± 0.10
10	95/5[d] -5CB	DMF/AcOH	35	10	1.08 ± 0.27	0.97 ± 0.15	0.94 ± 0.16

[a]Before thermostabilization.
[b]After thermostabilization.
[c]HKL/PEG = 99/1.
[d]HKL/PEG = 95/5.

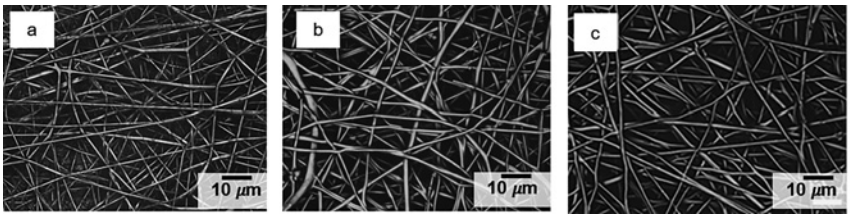

Figure 2: Microscopic images of lignin-based fiber mat prepared from HKL:PEG = 95:5 mixed with 10 wt% hexamine at 35 wt% in DMF/AcOH (6/4). The electrospun fiber mat (a); thermostabilized fiber (b) mat; activated fiber mat (c).

morphology of the electrospun lignin fiber mats was retained in the ACF mats even after carbonization and steam activation. The average diameters of thermostabilized mats and steam-activated ones are also summarized in Table 1. The fiber diameters in the mats were decreased by thermostabilization and steam-activation. Especially, the diameter decrement (27% on the intact mat) of the ACF-95/5 by these processes was much greater than that (14% on the intact mat) of the ACF-99/1, suggesting that PEG content affected the diameter of ACF mat.

For successful electrospinning of HKL/PEG-based ACF with CB, the CB (at 1 wt% and 5 wt%) was directly mixed with the HKL/PEG/hexamine solution, prior to electrospinning. However, this attempt was found impossible to perform due to the very high viscosity of the mixed solution and the existence of CB aggregate stucking in the syringe nozzle. Therefore, the strategy for CB deposition in the mat was changed to spraying a suspension of CB/acetone onto the electrospun mat during the electrospinning of HKL/PEG/hexamine (95/5/10) in DMF/AcOH (6/4). This spraying method seemed successful. SEM images of the ACF mats with and without spraying are shown in Figure 3. The CB-sprayed ACF mat (Figure 3c, d) clearly showed the existence of CB as particles in the mat.

In a separate experiment, the surface resistance of ACF-95/5 without CB, ACF-95/5-1CB, and ACF-95/5-5CB were measured to evaluate their performance as an electrode and found to be 901 ± 42.1 Ω, 164.7 ± 30.2 Ω, and 95.4 ± 11.8 Ω, respectively. The resistance dramatically decreased after the addition of CB, apparently depending on the CB content.

3.2 Characterizations of the ACFs

The elemental compositions of the ACF-95/5 and ACF-95/5-5CB are summarized in Supplementary Table S1. The 5.5 wt % increase in the carbon content of ACF-95/5-5CB confirmed the deposition of CB in ACF. The Raman spectra of ACF-95/5 and ACF-95/5-5CB are shown in Figure 4. The disordered carbon band (D-band) and graphitized carbon band (G-band) are clearly visible at 1340 and 1589 cm^{-1}, respectively (Dresselhaus et al. 2010). The I_D/I_G ratio (Dikio et al. 2013) of ACF-95/5 is estimated to be 0.95, while that of ACF-95/5-5CB is 0.96. Thus, the I_D/I_G ratios were identical, suggesting that CB did not affect the generation of graphitized carbon.

In Figure 5, the N_2 adsorption/desorption isotherms of ACF99/1 and ACF95/5 show narrow hysteresis loops, while ACF-95/5-1CB and -5CB show larger hysteresis loops compared to the corresponding ACF mats without CB. These results suggest the mesopores were developed with larger volumes for CB-embedded ACF mats, according to the physisorption isotherm recommendations of the IUPAC (Sing 1982).

Table 2 shows the BET specific surface areas (BSA), external and internal surface areas, pore size distributions, and total pore volumes calculated from the adsorption isotherms. For ACFs without CB, the BSA of ACF-95/5 was higher than that of ACF-99/1 under the same carbonization and steam activation conditions. In Figure 6 and Table 2, ACF-95/5 had slightly larger average pore size and volume in the micropore and mesopore regions compared to ACF-99/1. Therefore, the higher content of PEG resulted in larger

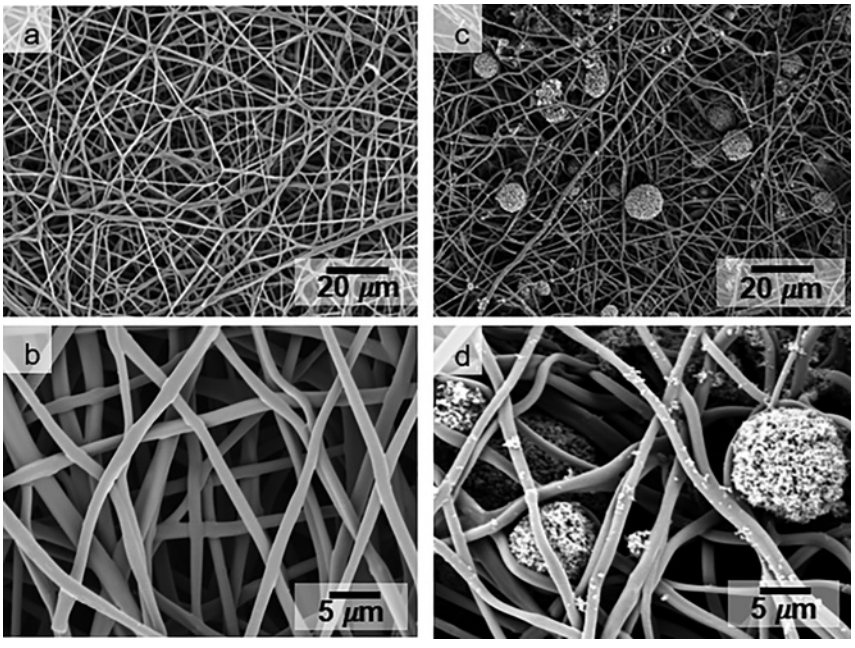

Figure 3: SEM image of ACF-95/5 mat (a, b) and ACF-95/5-5CB mat (c, d).

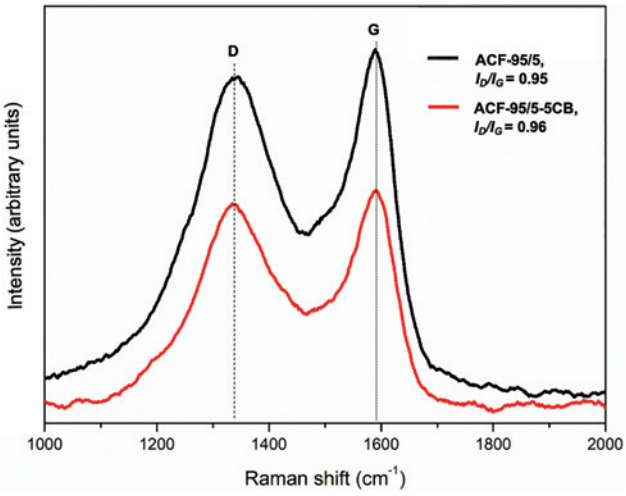

Figure 4: Raman spectra with I_D/I_G ratios of ACF 95/5 and ACF 95/5+5CB in the region of 1000–2000 cm^{-1}. The vertical dashed and dotted lines are guides for the eyes to indicate the positions of D- and G-bands, respectively.

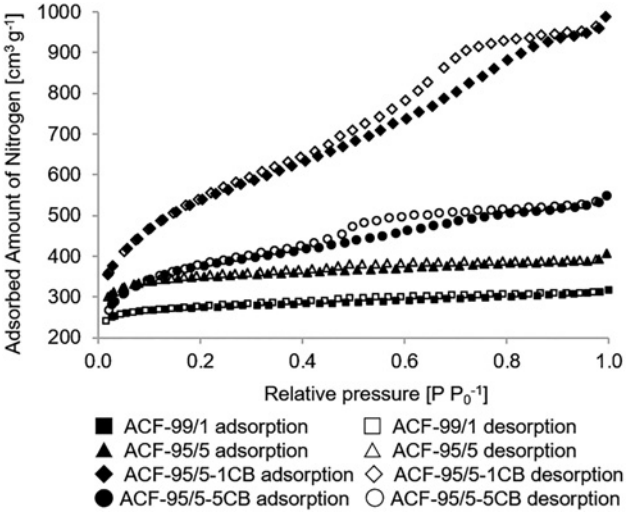

Figure 5: Adsorption and desorption isotherm of ACF-99/1, ACF-95/5, ACF-95/5-1CB, and ACF-95/5-5CB.

pores, which were expected to play an important role in the accumulation and transportation of IL electrolyte ions in the EDLCs. When CB was embedded into the ACF-95/5, all parameter values except the internal surface area in Table 2 increased. This result may be partly due to the CB providing vacant space between the fibers (Figure 3), allowing the steam to easily penetrate into the spaces to accelerate the steam activation. When the CB increased from 1 to 5 wt%, all the parameters decreased, while the internal surface area increased. Although the reason was not clear yet, the CB particles might have affected the activation process (Supplementary Table S2).

3.3 Electrochemical performance of EDLCs assembled with the electrospun HKL/PEG-based ACF mats

The ACF mats were cut into cylindrical shapes and directly used as electrodes with an IL ($EMIBF_4$) and an organic electrolyte ($TEMABF_4$) for EDLC to assemble separately. CV profiles for the resulting EDLCs were measured in a potential window of 0–3.5 V at a scan rate of 0.05 V s^{-1}, as shown in Figure 7. The CV profiles of the EDLC with $EMIBF_4$ (Figure 7a) showed an identical shape over 16–20 scan cycles, while the CV profiles of EDLC with $TEMABF_4$ (Figure 7b) for the same number of scan cycles did not overlap, especially at high voltage, indicating that $EMIBF_4$ was electrochemically stable in the potential range of 0–3.5 V. Thus, the advantage of IL electrolyte with wider potential window over organic electrolyte was confirmed (Mousavi et al. 2016).

Figure 8 includes CV profiles of EDLCs prepared using ACF-99/1 and ACF-95/5 with the IL electrolyte. The electrochemical performance calculated from the profiles is summarized in Table 3. The EDLC with ACF-95/5 (pink)

Table 2: N_2 adsorption/desorption properties of ACFs.

Samples	Surface area[a] (BSA) (m^2 g^{-1})	Pore volume (ml g^{-1})	Average pore diameter[b] (nm)		Internal surface area[c] (m^2 g^{-1})	External surface area[c] (m^2 g^{-1})
			Micropore area	Mesopore area		
ACF-99/1	854	0.44	0.87 (97.2%)	3.04 (2.8%)	763	91
ACF-95/5	1091	0.56	0.89 (97.2%)	2.96 (2.8%)	971	120
ACF-95/5-1CB	1509	1.07	1.17 (69.8%)	3.19 (30.2%)	509	1000
ACF-95/5-5CB	1235	0.75	1.03 (84.4%)	3.04 (15.6%)	798	438

[a]Calculated by the BET model.
[b]Calculated based on QSDFT model.
[c]Calculated according to *t*-plot method.

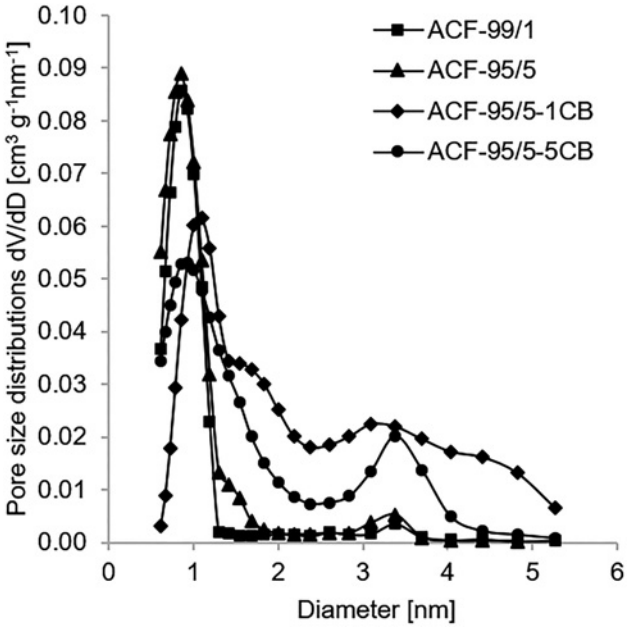

Figure 6: Pore size distribution of ACF with/without CB.

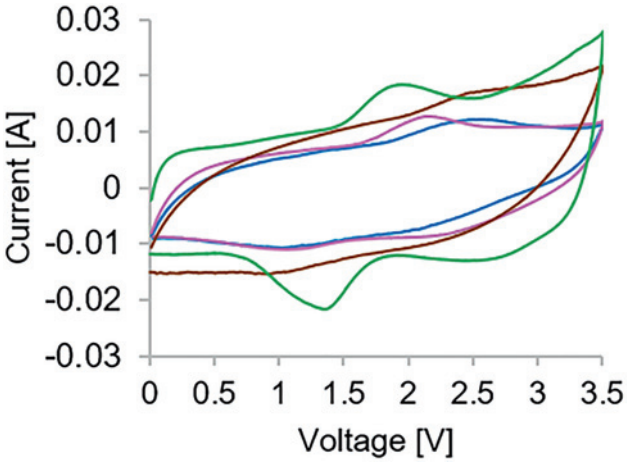

Figure 8: Average cyclic voltammograms of ACF electrode prepared from ACF-99/1 (blue), ACF-95/5 (pink), ACF-95/5-1CB (brown) and ACF-95/5-5CB (green) measured for 1–15 cycles in air. All samples were measured at scan rate 0.05 V s^{-1}.

showed a bigger CV area (Figure 8), leading to its higher capacitance than that with ACF-99/1 (blue). The higher capacitance was attributed to the higher BSA and the larger pore size of the ACF-95/5 electrode (Table 2), which provides more space for electron accumulation and transportation.

The CV profiles of ACF-99/1 and ACF-95/5 showed a bow-like shape with an oxidation peak at 1.5–3.0 V and a reduction peak at 1.65–2.5 V. These profiles indicated the obtained EDLCs were categorized as pseudocapacitors, rather than simple EDLCs. The reason for the occurrence of redox reactions is discussed in a later section. Figure 9 and Table 3 show the GCD profiles of EDLC-99/1 and EDLC-95/5 at a current density of 1 A g^{-1} and the electrochemical performance calculated from the GCD profiles, respectively. The GCD (158.7 F g^{-1}) and CV (149.8 F g^{-1}) capacitances of the EDLC from ACF-95/5 were comparable to those of commercial electrodes for supercapacitors (Murayama et al.

Table 3: Electrochemical performance of the EDLCs prepared with various ACF electrodes at voltage window of 0–3.5 V in ionic liquid electrolyte measured in an air atmosphere.

EDLC-samples	C_{sp} [a] (F g^{-1})	C_{sp} [b] (F g^{-1})	R_c [c] (Ω)	R_i [d] (Ω)	Energy density (Wh kg^{-1})	Power density (kW kg^{-1})
EDLC-99/1	82.9	76.0	18.5	3.5	32.3	1.9
EDLC-95/5	149.8	158.7	16.1	1.6	67.5	11.5
EDLC-95/5-1CB	114.9	156.3	11.4	1.7	66.5	59.5
EDLC-95/5-5CB	176.8	227.3	2.8	1.9	91.5	76.2

[a]Calculated by CV method.
[b]Calculated by GCD method.
[c]Charge transfer resistance.
[d]Intrinsic resistance.

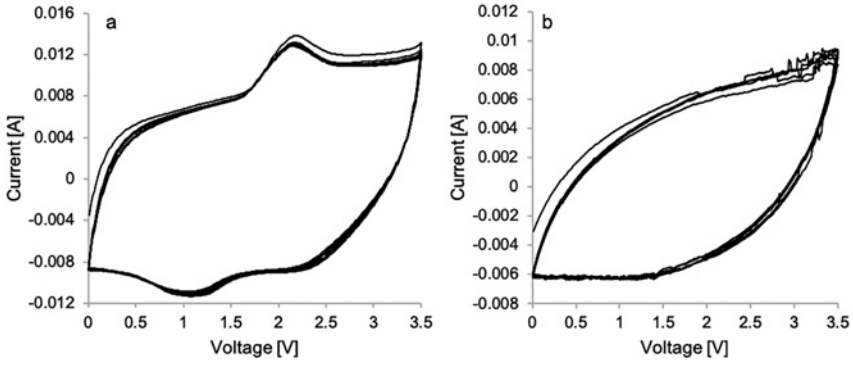

Figure 7: Cyclic voltammograms of EDLC prepared from ACF-95/5 with different electrolyte at potential window 0–3.5 V and scan rate 0.05 V s^{-1} in 16–20 scan cycles. IL electrolyte ($EMIBF_4$) (a); organic electrolyte ($TEMABF_4$) (b).

2005; Shiraishi et al. 2007; Soeda et al. 2015) and much larger than those of ACF-99/1. However, a large Vdrop was observed in the discharge process in its GCD (pink in Figure 9). In addition, a relatively large charge transfer resistance (R_c) was revealed by EIS measurements (pink in Figure 10 and 16.1 Ω in Table 3). Consequently, the wide potential window and high capacitance resulted in significantly high energy density (67.5 Wh kg^{-1}), but the large V_{drop} caused low power density (11.5 kW kg^{-1}). The reason for the low power density might be due to the low conductivity of the electrode. Therefore, an improvement of the electrode conductivity was attempted by adding conductive CB to ACF mats.

Figure 8 also includes CV profiles of EDLCs prepared from ACF-95/5-1CB and -5CB with IL electrolyte. The electrochemical parameters obtained from Figure 8 are listed in Table 3. The addition of 1 wt% CB to the HKL/PEG/HEX-electrospun mat (ratio of 95/5/10) decreased the specific capacitances calculated from both the CV and GCD measurements (Table 3), even though the BSA was increased by the addition of CB (Table 2). Therefore, the reduction must be attributed to the decrease of the internal surface area (Table 2), which is directly related to the adsorption of the adsorbate (Mao et al. 2018). By contrast, the addition of 5 wt % CB drastically increased the specific capacitance because the internal surface area of ACF-95/5-5CB was much larger than ACF-95/5-1CB.

In Figure 9, the V_{drop} in the GCD profiles of EDLC-95/5-1CB and -5CB were smaller than those of EDLC-99/1 and EDLC-95/5, and EDLC-95/5-5CB had a smaller V_{drop} than -1CB. According to the power density equation, the EDLC with ACF-95/5-5CB had higher power density than -1CB, since V_{max} and i were identical. As shown in Table 3, its large capacitance calculated from the GCD profile (227.3 F g^{-1}) resulted in the highest energy density (91.5 Wh kg^{-1}). Besides, it turned out from an analysis of Nyquist plots (Figure 10) that the R_c of ACF-95/5-5CB decreased dramatically to 2.8 Ω, resulting in high capacitance and energy density (Lei et al. 2013; Zuliani et al. 2013). Therefore, the addition of 5 wt% CB enhanced both the energy and power densities.

Figure 11 shows changes in the specific capacitance over 100 GCD cycles. The capacitance of EDLC-95/5-5CB decreased to 60% (135.1 F g^{-1}) of its original capacitance at the 100th cycle. In addition, the CV profiles of this EDLC during cycles 10–40 with redox peaks did not overlap (Supplementary Figure S1a), suggesting instability of the EDLC under measurement condition in the air (RH 25 ± 3%). This instability was assumed to be caused by moisture, which may penetrate to the measurement cell during the experiment through insufficient insulation (Cericola et al. 2011; Welton 1999; Yang et al. 2016). To confirm the assumption, the electrochemical performance of EDLC-95/5-5CB was measured in an argon chamber, where the RH was maintained at 5 ± 2%. The CV profile in the argon atmosphere showed a smaller redox peak than that of the peak seen in the air (Supplementary Figure S1b). Therefore, it was confirmed that moisture caused the redox reaction with the IL electrolyte. As a result, the GCD specific capacitance after

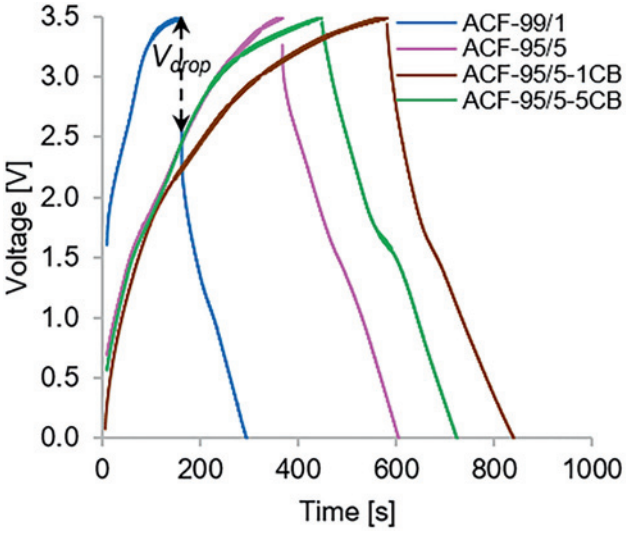

Figure 9: Galvanostatic charge–discharge curves of various ACF electrode types at 0–3.5 V. All samples were measured at current density of 1 A g^{-1} in ambient condition and using IL as an electrolyte.

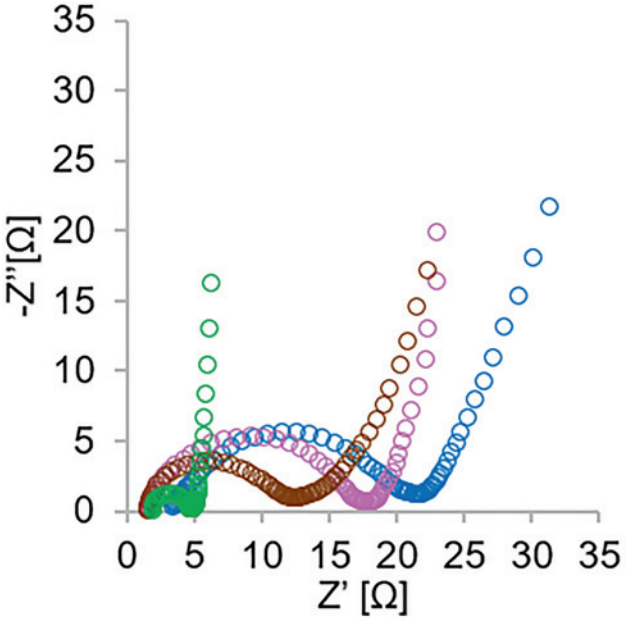

Figure 10: Nyquist plots of ACF electrode prepared from ACF-99/1 (blue), ACF-95/5 (pink), ACF-95/5-1CB (brown) and ACF-95/5-5CB-based EDLCs (green).

100 cycles was retained at 80% (184.2 F g^{-1}) of that at the first cycle in the argon atmosphere (Figure 11). Additionally, the energy density and power density were increased from 57.5 Wh kg^{-1} to 78.3 Wh kg^{-1} and from 54.7 kW kg^{-1} to 62.1 kW kg^{-1}, respectively, by changing the measurement atmosphere from air to argon (data not shown in Table 3).

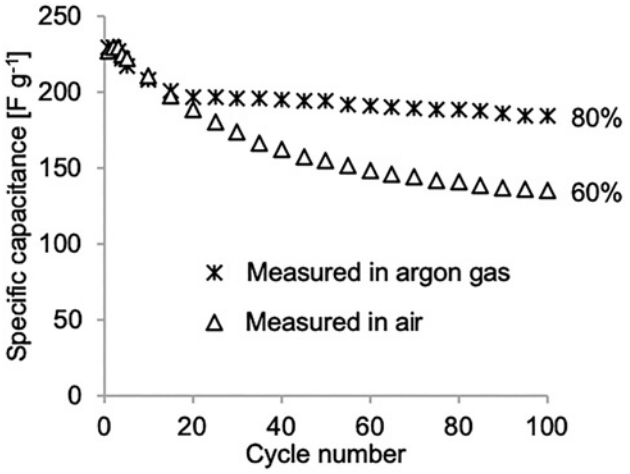

Figure 11: Change in specific capacitance of ACF-95/5-5CB over cycling from GCD at current density of 1 A g^{-1} that measured separately in air and in argon gas.

For practical use of EDLC, the moisture effect is not considered so serious a problem because commercial EDLC cells are tightly packed in inert gas.

The comparison of specific capacitance, energy density, and power density report in several recent studies about lignin-based EDLC with IL electrolyte in the two-electrode system are listed in Table 4. While specific capacitance by some researches is high (e. g., over 200 F g^{-1}), the energy (E) and power (P) densities are not as impressive (Table 4). For instance, Zhang et al. (2019) reported specific capacitance at 289 F g^{-1} at 1 A g^{-1}, while E and P were 66.2 Wh kg^{-1} and 0.31 W kg^{-1}, respectively. The lower E and P could be attributed to their operating voltage window of 2.5 V, which was narrower than that used in this research work (3.5 V). Therefore, as far as our knowledge goes, the lignin-based electrode with IL electrolyte of the current work achieved the highest reported energy density of the EDLC (91.5 Wh kg^{-1}) ever reported.

The advantages of the use of CB have been described so far. However, the electrode with high electrostatic capacitance was not successfully fabricated only with CB, as shown in the CV plot of Supplementary Figure S2a. Therefore, the insertion of CB in lignin electrospun lignin fiber mats is the prerequisite to fabricate a high electrochemical performance EDLC.

Table 4: Comparison of electrochemical performances of lignin-based EDLC in ionic liquid electrolyte in two-electrode system.

Carbon electrode	Electrolyte	Specific capacitance (F g^{-1})	Energy density (Wh kg^{-1})	Power density[a] (kW kg^{-1})	References
Alkali lignin derived ACNF:PVA	Pyr_{14}TFSI in PC and EC[b]	88 at 0.01 V s^{-1}	38	1.67	Jayawickramage and Ferraris 2019
Alkali Kraft lignin derived ACNF:-PAN	Pyr_{14}TFSI in PC and EC[b]	128 at 0.01 V s^{-1}	59	15	Jayawickramage et al. 2019
Lignin waste derived activated carbons	BMI BF_4[c]	175 at 0.5 A g^{-1}	16.4	15	Sangchoom et al. 2018
Enzymatic hydrolysis lignin derived hierarchical porous carbon	EMI TFSI[d]	218 at 1 A g^{-1}	46.8	25.4	Guo et al. 2017
Alkali lignin -derived porous carbon (bacteria-activation)	EMI TFSI[d]	289 at 1 A g^{-1}	66.2	0.32	Zhang et al. 2019
Lignin derived double-capillary carbon nanofibers	EMI BF_4[e]	133 at 1 A g^{-1}	56.6	1.76	Wang et al. 2016
Softwood kraft lignin derived porous carbon	EMI BF_4[e]	231 at 1 A g^{-1}	No report	No report	Klose et al. 2017
Hardwood Kraft lignin derived ACF:PEG	EMI BF_4[e]	227.3 at 1 A g^{-1}	91.5	76.2	This work

[a]Power density could be derived at a curtain energy density.
[b]Pyr_{14}TFSI in PC and EC = N-methyl pyrrolidinium bis(trifluoromethanesulfonyl)imide (Pyr_{14}TFSI) dissolved in a mixture of propylene carbonate (PC) and ethylene carbonate (EC).
[c]BMI BF_4 = 1-butyl-3-methylimidazolium tetrafluoroborate.
[d]EMI TFSI = 1-ethyl-3-methylimidazolium bis(trifluoromethylsulfonyl)imide.
[e]EMI BF_4 = 1-ethyl-3-methylimidazolium tetrafluoroborate.

4 Conclusions

Although it took 8 h to thermostabilize the electrospun fiber mat of HKL/PEG, the addition of Hex greatly shortened the thermostabilization time to 2 h. In addition, the CB addition to the mat dramatically improved the electrochemical performance of the ACF mat as an EDLC electrode due to the generation of larger pores suitable for IL electrolyte and lower electric conductivity. Consequently, the EDLC with high energy density (91.5 Wh kg^{-1}) and power density (76.2 kW kg^{-1}) has successfully fabricated. For the practical use of future EDLC termed as a supercapacitor, the large electrostatic capacitance, energy density and power density based on a pair of electrodes or a unit cell are required, although the present study demonstrated the excellent electrochemical performance based on the weight of electrode material. To achieve these requirements, the multilamination of the ACF mat on a single electrode is under investigation.

As lignin-based separators have been developed for an organic electrolyte of EDLC (Koda et al. 2019; Taira et al. 2019), a future target is the fabrication of EDLC with IL electrolyte from lignin-based electrode and separator.

Acknowledgments: We are grateful to Machinery Lab. of the Institute for Catalysis, Hokkaido University, for preparing a container for thermostabilization of electrospun lignin mat.

Author contribution: All the authors have accepted responsibility for the entire content of this submitted manuscript and approved submission.

Research funding: This work was supported by JSPS KAKENHI Grant Number JP19J22306.

Employment or leadership: None declared.

Honorarium: None declared.

Conflict of interest statement: The authors declare no conflicts of interest regarding this article.

References

Ago, M., Borghei, M., Haataja, J.S., and Rojas, O.J. (2016). Mesoporous carbon soft-templated from lignin nanofiber networks: microphase separation boosts supercapacitance in conductive electrodes. RSC Adv. 6: 85802–85810, https://doi.org/10.1039/C6RA17536H.

Aso, T., Koda, K., Kubo, S., Yamada, T., Nakajima, I., and Uraki, Y. (2013). Preparation of novel lignin-based cement dispersants from isolated lignins. J. Wood Chem. Technol. 33: 286–298, https://doi.org/10.1080/02773813.2013.794841.

Braun, J.L., Holtman, K.M., and Kadla, J.F. (2005). Lignin-based carbon fibers: oxidative thermostabilization of kraft lignin. Carbon 43: 385–394, https://doi.org/10.1016/j.carbon.2004.09.027.

Cericola, D., Ruch, P., Foelske-Schmitz, A., Weingarth, D., Kötz, R., (2011). Effect of water on the aging of activated carbon based electrochemical double layer capacitors during constant voltage load tests. Int. J. Electrochem. Sci. 6, 988–996. https://journals.indexcopernicus.com/search/details?id=8778.

Chmiola, J., Yushin, G., Gogotsi, Y., Portet, C., Simon, P., and Taberna, L.P. (2006). Anomalous increase in carbon capacitance at pore sizes less than 1 nanometer. Science 313: 1760–1763, https://doi.org/10.1126/science.1132195.

Cline, S.P. and Smith, P.M. (2017). Opportunities for lignin valorization: an exploratory process. Energy Sustain. Soc. 7: 26, https://doi.org/10.1186/s13705-017-0129-9.

Daraghmeh, A., Hussain, S., Saadeddin, I., Servera, L., Xuriguera, E., Cornet, A., and Cirera, A. (2017). A study of carbon nanofibers and active carbon as symmetric supercapacitor in aqueous electrolyte: a comparative study. Nanoscale Res. Lett. 12: 639, https://doi.org/10.1186/s11671-017-2415-z.

De Vos, N., Maton, C., and Stevens, C.V. (2014). Electrochemical stability of ionic liquids: general influences and degradation mechanisms. ChemElectroChem 1: 1258–1270, https://doi.org/10.1002/celc.201402086.

Den, W., Sharma, V.K., Lee, M., Nadadur, G., and Varma, R.S. (2018). Lignocellulosic biomass transformations via greener oxidative pretreatment processes: access to energy and value-added chemicals. Front. Chem. 6: 141, https://doi.org/10.3389/fchem.2018.00141.

Deng, L., Young, R.J., Kinloch, I.A., Abdelkader, A.M., Holmes, S.M., Rio, D.A.D.H.D., and Eichhorn, S.J. (2013). Supercapacitance from cellulose and carbon nanotube nanocomposite fibers. ACS Appl. Mater. Interfaces 5: 9983-9990, https://doi.org/10.1021/am403622v.

Dikio, E.D., Shooto, N.D., Thema, F.T., and Farah, A.M. (2013). Raman and TGA study of carbon nanotubes synthesized over Mo/Fe catalyst on aluminium oxide, calcium carbonate and magnesium oxide support. Chem. Sci. Trans. 2: 1160–1173, https://doi.org/10.7598/cst2013.519.

Dresselhaus, M.S., Jorio, A., Hofmann, M., Dresselhaus, G., and Saito, R. (2010). Perspectives on carbon nanotubes and graphene raman spectroscopy. Nano Lett. 10: 751–758, https://doi.org/10.1021/nl904286r.

Espinoza-Acosta, J.L., Torres-Chávez, P.I., Olmedo-Martínez, J.L., Vega-Rios, A., Flores-Gallardo, S., and Zaragoza-Contreras, E.A. (2018). Lignin in storage and renewable energy applications: a review. J. Energy Chem. 27: 1422–1438, https://doi.org/10.1016/j.jechem.2018.02.015.

Ganewatta, M.S., Lokupitiya, H.N., and Tang, C. (2019). Lignin biopolymers in the age of controlled polymerization. Polymers 11: 1176, https://doi.org/10.3390/polym11071176.

Gao, Q., Demarconnay, L., Raymundo-Piñero, E., and Béguin, F. (2012). Exploring the large voltage range of carbon/carbon supercapacitors in aqueous lithium sulfate electrolyte. Energy Environ. Sci. 5: 9611, https://doi.org/10.1039/C2EE22284A.

Guo, N., Li, M., Sun, X., Wang, F., and Yang, R. (2017). Enzymatic hydrolysis lignin derived hierarchical porous carbon for supercapacitors in ionic liquids with high power and energy densities. Green Chem. 19: 2595–2602, https://doi.org/10.1039/C7GC00506G.

Hayyan, M., Mjalli, F.S., Hashim, M.A., AlNashef, I.M., and Mei, T.X. (2013). Investigating the electrochemical windows of ionic liquids. J. Ind. Eng. Chem. 19: 106–112, https://doi.org/10.1016/j.jiec.2012.07.011.

Jayawickramage, R.A.P. and Ferraris, J.P. (2019). High performance supercapacitors using lignin based electrospun carbon nanofiber electrodes in ionic liquid electrolytes. Nanotechnology 30: 155402, https://doi.org/10.1088/1361-6528/aafe95.

Jayawickramage, R.A.P., Balkus, K.J., and Ferraris, J.P. (2019). Binder free carbon nanofiber electrodes derived from polyacrylonitrile-lignin blends for high performance supercapacitors. Nanotechnology 30: 355402, https://doi.org/10.1088/1361-6528/ab2274.

Kadla, J.F., Kubo, S., Venditti, R.A., Gilbert, R.D., Compere, A.L., and Griffith, W. (2002). Lignin-based carbon fibers for composite fiber applications. Carbon 40: 2913–2920, https://doi.org/10.1016/s0008-6223(02)00248-8.

Kim, T., Jung, G., Yoo, S., Suh, K.S., and Ruoff, R.S. (2013). Activated graphene-based carbons as supercapacitor electrodes with macro- and mesopores. ACS Nano 7: 6899–6905, https://doi.org/10.1021/nn402077v.

Kiseleva, E.A., Zhurilova, M.A., Kochanova, S.A., Shkolnikov, E.J., Tarasenko, A.B., Zaitseva, O.V., Uryupina, O.V., and Valyano, G.V. (2018). Influence of carbon conductive additives on electrochemical double-layer supercapacitor parameters. J. Phys. Conf. Ser. 946: 012030, https://doi.org/10.1088/1742-6596/946/1/012030.

Klose, M., Reinhold, R., Logsch, F., Wolke, F., Linnemann, J., Stoeck, U., Oswald, S., Uhlemann, M., Balach, J., Markowski, J., et al. (2017). Softwood lignin as a sustainable feedstock for porous carbons as active material for supercapacitors using an ionic liquid electrolyte. ACS Sustain. Chem. Eng. 5: 4094–4102, https://doi.org/10.1021/acssuschemeng.7b00058.

Koda, K., Taira, S., Kubota, A., Isozaki, T., You, X., Uraki, Y., Sugimura, K., and Nishio, Y. (2019). Development of lignin-based terpolyester film and its application to separator material for electric double-layer capacitor. J. Wood Chem. Technol. 39: 198–213, https://doi.org/10.1080/02773813.2018.1562472.

Kołodyńska, D., Gęca, M., Pylypchuk, I.V., and Hubicki, Z. (2016). Development of new effective sorbents based on nanomagnetite. Nanoscale Res. Lett. 11: 152, https://doi.org/10.1186/s11671-016-1371-3.

Kumar, M., Hietala, M., and Oksman, K. (2019). Lignin-based electrospun carbon nanofibers. Front. Mater. 6: 62, https://doi.org/10.3389/fmats.2019.00062.

Lei, C., Markoulidis, F., Ashitaka, Z., and Lekakou, C. (2013). Reduction of porous carbon/Al contact resistance for an electric double-layer capacitor (EDLC). Electrochim. Acta 92: 183–187, https://doi.org/10.1016/j.electacta.2012.12.092.

Lei, D., Li, X.D., Seo, M.K., Khil, M.S., Kim, H.Y., and Kim, B.S. (2017). $NiCo_2O_4$ nanostructure-decorated PAN/lignin based carbon nanofiber electrodes with excellent cyclability for flexible hybrid supercapacitors. Polymer 132: 31–40, https://doi.org/10.1016/j.polymer.2017.10.051.

Lora, J. (2008). Industrial commercial lignins: sources, properties and applications. In: Belgacem, M.N., and Gandini, A. (Eds.). *Monomers, polymers and composites from renewable resources*. Elsevier, Amsterdam, pp. 225–241.

Luo, J., Genco, J., Cole, B., and Fort, R. (2011). Lignin recovered from the near-neutral hemicellulose extraction process as a precursor for carbon fiber. Bioresources 6: 4566–4593.

Mao, Z.X., Wang, C., Shan, Q., Wang, M.J., Zhang, Y., Ding, W., Chen, S., Li, L., Li, J., and Wei, Z. (2018). An unusual low-surface-area nitrogen doped carbon for ultrahigh gravimetric and volumetric capacitances. J. Mater. Chem. 6: 8868–8873, https://doi.org/10.1039/C8TA02198H.

Mhamane, D., Suryawanshi, A., Banerjee, A., Aravindan, V., Ogale, S., and Srinivasan, M. (2013). Non-aqueous energy storage devices using graphene nanosheets synthesized by green route. AIP Adv. 3: 042112, https://doi.org/10.1063/1.4802243.

Milotskyi, R., Szabó, L., Takahashi, K., and Bliard, C. (2019). Chemical modification of plasticized lignins using reactive extrusion. Front. Chem. 7: 633, https://doi.org/10.3389/fchem.2019.00633.

Mousavi, M.P.S., Wilson, B.E., Kashefolgheta, S., Anderson, E.L., He, S., Bühlmann, P., and Stein, A. (2016). Ionic liquids as electrolytes for electrochemical double-layer capacitors: structures that optimize specific energy. ACS Appl. Mater. Interfaces 8: 3396–3406, https://doi.org/10.1021/acsami.5b11353.

Murayama, I., Yoshimoto, N., Egashira, M., Morita, M., Kobayashi, Y., and Ishikawa, M. (2005). Characteristics of electric double layer capacitors with an ionic liquid electrolyte containing Li ion. Electrochemistry 73: 600–602, https://doi.org/10.5796/electrochemistry.73.600.

Neimark, A.V., Lin, Y., Ravikovitch, P.I., and Thommes, M. (2009). Quenched solid density functional theory and pore size analysis of micro-mesoporous carbons. Carbon 47: 1617–1628, https://doi.org/10.1016/j.carbon.2009.01.050.

Norberg, I., Nordström, Y., Drougge, R., Gellerstedt, G., and Sjöholm, E. (2012). A new method for stabilizing softwood kraft lignin fibers for carbon fiber production. J. Appl. Polym. Sci. 128: 3824–3830, https://doi.org/10.1002/app.38588.

Pandit, B., Dubal, D.P., and Sankapal, B.R. (2017). Large scale flexible solid state symmetric supercapacitor through inexpensive solution processed V_2O_5 complex surface architecture. Electrochim. Acta 242: 382–389, https://doi.org/10.1016/j.electacta.2017.05.010.

Park, J.H., Rana, H.H., Lee, J.Y., and Park, H.S. (2019). Renewable flexible supercapacitors based on all-lignin-based hydrogel electrolytes and nanofiber electrodes. J. Mater. Chem. A 7: 16962–16968, https://doi.org/10.1039/C9TA03519B.

Ramachandran, R. and Wang, F. (2018). Electrochemical capacitor performance: influence of aqueous electrolytes. In: Liudvinavicius, L. (Ed.). *Supercapacitors – theoretical and practical solutions*. InTech, London, UK, pp. 52–68.

Saha, D., Li, Y., Bi, Z., Chen, J., Keum, J.K., Hensley, D.K., Grappe, H.A., Meyer, H.M., Dai, S., Paranthaman, M.P., et al. (2014). Studies on supercapacitor electrode material from activated lignin-derived mesoporous carbon. Langmuir 30: 900–910, https://doi.org/10.1021/la404112m.

Salmani, L. and Nouri, M. (2016). Electrospun silk fibroin nanofibers with improved surface texture. J. Text. Polym. 4: 75.

Sangchoom, W., Walsh, D.A., and Mokaya, R. (2018). Valorization of lignin waste: high electrochemical capacitance of lignin-derived carbons in aqueous and ionic liquid electrolytes.

J. Mater. Chem. A, 6: 18701–18711, https://doi.org/10.1039/C8TA07632D.

Shiraishi, S., Miyauchi, T., Sasaki, R., Nishina, N., Oya, A., and Hagiwara, R. (2007). Electric double layer capacitance of activated carbon nanofibers in ionic liquid: $EMImBF_4$. Electrochemistry 75: 619–621, https://doi.org/10.5796/electrochemistry.75.619.

Sing, K.S.W. (1982). Reporting physisorption data for gas/solid systems with special reference to the determination of surface area and porosity (provisional). Pure Appl. Chem. 54: 2201–2218, https://doi.org/10.1351/pac198254112201.

Sixta, H. (2008). *Handbook of pulp*. Wiley-VCH Verlag, Weinheim.

Soeda, K., Yamagata, M., and Ishikawa, M. (2015). Outstanding features of alginate-based gel electrolyte with ionic liquid for electric double layer capacitors. J. Power Sources 280: 565–572, https://doi.org/10.1016/j.jpowsour.2015.01.144.

Szabó, L., Milotskyi, R., Fujie, T., Tsukegi, T., Wada, N., Ninomiya, K., and Takahashi, K. (2019). Short carbon fiber reinforced polymers: utilizing lignin to engineer potentially sustainable resource-based biocomposites. Front. Chem. 7, https://doi.org/10.3389/fchem.2019.00757.

Taira, S., Kurihara, M., Koda, K., Sugimura, K., Nishio, Y., and Uraki, Y. (2019). TEMPO-oxidized cellulose nanofiber-reinforced lignin based polyester films as a separator for electric double-layer capacitor. Cellulose 26: 569–580, https://doi.org/10.1007/s10570-018-2101-z.

Thakur, V.K., Thakur, M.K., Raghavan, P., and Kessler, M.R. (2014). Progress in green polymer composites from lignin for multifunctional applications: a review. ACS Sustain. Chem. Eng. 2: 1072–1092, https://doi.org/10.1021/sc500087z.

Tuck, C.O., Perez, E., Horvath, I.T., Sheldon, R.A., and Poliakoff, M. (2012). Valorization of biomass: deriving more value from waste. Science 337: 695–699, https://doi.org/10.1126/science.1218930.

Uraki, Y., Kubo, S., Nigo, N., Sano, Y., and Sasaya, T. (1995). Preparation of carbon fibers from organosolv lignin obtained by aqueous acetic acid pulping. Holzforschung 49: 343–350, https://doi.org/10.1515/hfsg.1995.49.4.343.

Uraki, Y., Nakatani, A., Kubo, S., and Sano, Y. (2001). Preparation of activated carbon fibers with large specific surface area from softwood acetic acid lignin. J. Wood Sci. 47: 465–469, https://doi.org/10.1007/bf00767899.

Wang, J., Tang, J., Xu, Y., Ding, B., Chang, Z., Wang, Y., Hao, X., Dou, H., Kim, J.H., Zhang, X., et al. (2016). Interface miscibility induced double-capillary carbon nanofibers for flexible electric double layer capacitors. Nano Energy 28: 232–240, https://doi.org/10.1016/j.nanoen.2016.08.043.

Wang, X., Li, Y., Lou, F., Buan, M.E.M., Sheridan, E., and Chen, D. (2017). Enhancing capacitance of supercapacitor with both organic electrolyte and ionic liquid electrolyte on a biomass-derived carbon. RSC Adv. 7: 23859–23865, https://doi.org/10.1039/C7RA01630A.

Welton, T. (1999). Room-temperature ionic liquids. Solvents for synthesis and catalysis. Chem. Rev. 99: 2071–2084, https://doi.org/10.1021/cr980032t.

Yang, C.S., Shang, D.S., Chai, Y.S., Yan, L.Q., Shen, B.G., and Sun, Y. (2016). Moisture effects on the electrochemical reaction and resistance switching at Ag/molybdenum oxide interfaces. Phys. Chem. Chem. Phys. 18: 12466–12475, https://doi.org/10.1039/C6CP00823B.

You, X., Koda, K., Yamada, T., and Uraki, Y. (2015). Preparation of electrode for electric double layer capacitor from electrospun lignin fibers. Holzforschung 69: 1097–1106, https://doi.org/10.1515/hf-2014-0262.

You, X., Koda, K., Yamada, T., and Uraki, Y. (2016a). Preparation of high-performance internal tandem electric double-layer capacitors (IT-EDLCs) from melt-spun lignin fibers. J. Wood Chem. Technol. 36: 418–431, https://doi.org/10.1080/02773813.2016.1212893.

You, X., Duan, J., Koda, K., Yamada, T., and Uraki, Y. (2016b). Preparation of electric double layer capacitors (EDLCs) from two types of electrospun lignin fibers. Holzforschung 70: 661–671, https://doi.org/10.1515/hf-2015-0175.

Zhang, K., Liu, M., Zhang, T., Min, X., Wang, Z., Chai, L., and Shi, Y. (2019). High-performance supercapacitor energy storage using a carbon material derived from lignin by bacterial activation before carbonization. J. Mater. Chem. A 7: 26838–26848, https://doi.org/10.1039/C9TA04369A.

Zuliani, E.J., Zereen, M., Charles, Q.J., Donald, W.K. (2013). Effects of temperature on electrochemical double layer capacitor performance using activated carbon electrodes. In: *223rd ECS meeting*. The Electrochemical Society, Canada.

Supplementary Material: The online version of this article offers supplementary material (https://doi.org/10.1515/hf-2019-0291).